Journal of Power Sources 257 (2014) 65–69

Contents lists available at ScienceDirect

Journal of Power Sources

journal homepage: www.elsevier.com/locate/jpowsour

Short communication

Direct growth of $FePO_4$/graphene and $LiFePO_4$/graphene hybrids for high rate Li-ion batteries

Qi Fan [a,*], Lixu Lei [a], Xingyu Xu [b,c], Gui Yin [d], Yueming Sun [a,*]

[a] School of Chemistry and Chemical Engineering, Southeast University, Nanjing 211189, China
[b] Department of Physics, Southeast University, Nanjing 211189, China
[c] MEMS Key Laboratory of Education Ministry, Department of Electrical Engineering, Southeast University, Nanjing 210096, China
[d] Huaan High-Tech Research Institute of Nanjing University, Huaian 223003, China

HIGHLIGHTS

- $FePO_4$/graphene and $LiFePO_4$/graphene hybrids were synthesized by a simple method.
- A simple and environmentally friendly RAAP-induced growth method was used.
- $FePO_4$ and $LiFePO_4$ were direct grown on the graphene-assembled scaffolds.
- $FePO_4$/graphene hybrids present superior electrochemical properties.
- $LiFePO_4$/graphene hybrids present superior electrochemical properties.

ARTICLE INFO

Article history:
Received 1 November 2013
Received in revised form
27 December 2013
Accepted 9 January 2014
Available online 18 January 2014

Keywords:
Iron phosphate
Lithium iron phosphate
Direct growth
Graphene
Cathode
Li-ion battery

ABSTRACT

$FePO_4$/graphene and $LiFePO_4$/graphene hybrids have been synthesized by an eco-friendly RAAP-directed growth method. With this strategy, $FePO_4$ and $LiFePO_4$ particles have been grown on the exfoliated graphene-assembled scaffolds. Both of the hybrids present superior electrochemical properties, i.e., high rate capability combined with good capacity retention upon cycling, indicating the great potential as the cathode materials for Li-ion batteries.

1. Introduction

Due to the significant requirements of renewable green energy technology, Li-ion battery(LIB)becomes the predominant power source for home electronics and large-scale energy storage devices [1,2]. Developing new cathode materials which deliver more energy density is important for us to achieve better LIBs [3–8]. Among various cathode materials, phosphate ion-based materials ($LiFePO_4$ and $FePO_4$) come into prominence with regard to their relatively high theoretical capacity, excellent cycling performance, low cost, nontoxicity, environmental friendliness and safe nature, leading to strong focus on polyanionic chemistries [4,9–17]. However, both of the two cathode materials suffer from poor electronic conductivity and poor transport, resulting in reduced utilization at high charge/discharge rates. A common solution is to use carbon nanotubes (CNTs) and graphene as carriers for insulating $LiFePO_4$ or $FePO_4$ nanoparticles, because both can produce highly conductive networks in the cathodes [12,18–22]. In order to improve the dispersity of the carbon material and modify the connection between the active materials and the carriers, CNTs and graphene were usually pre-oxidized in the synthesize process. However, such processing destroys the intact structures of carbon materials, leading to the relatively low utilization of the active materials.

Herein, a facile synthesize method was developed to grow the $FePO_4$ and $LiFePO_4$ particles on the thermally exfoliated graphene-

* Corresponding authors. Fax: +86 25 8679 2637.
E-mail addresses: fanqi1984@126.com (Q. Fan), Sun@seu.edu.cn (Y. Sun).

0378-7753/$ – see front matter © 2014 Elsevier B.V. All rights reserved.
http://dx.doi.org/10.1016/j.jpowsour.2014.01.044

sheets (TGs). Rhodanineacetic acid-pyrene (RAAP) was used to functionalize the graphene nanosheets to induce the growth of $FePO_4$ particles on the graphene nanosheets, and then thermal reduction method was used to transform the $FePO_4$/graphene to $LiFePO_4$/graphene hybrids. Both of the fabricated composites were used as the cathodes in Li-ion batteries which exhibit superior performance, i.e., high rate capability combined with good capacity retention upon cycling.

2. Experimental

In a typical synthesis, Thermally exfoliated graphene nanosheets (TGs) with large specific surface area were obtained by the method of thermal treating graphite oxide at 700 °C in N_2 for 2 h. As-synthesized TGs were selected to prepare $FePO_4$/graphene and $LiFePO_4$/graphene hybrids (Scheme 1) [23]. They (0.4 g TGs) were well dispersed into the dimethylformamide (DMF)/water solution (1:1, 500 ml) with the dispersant RAAP (0.08 g). As the strong π–π stacking force between the RAAP and TGs, RAAP molecules were well decorated on the TGs. Due to their strong hydrophilicity, TGs can be easily separated from each other and the surface of them became negative charged (Scheme 1b). Then, $FeSO_4{\cdot}7H_2O$ (1.5 M, 25 ml) and $(NH_4)H_2PO_4$ (1.5 M, 25 ml) solution were added drop-by-drop sequentially with vigorous stirring. Since the effect as heterogeneous charges attraction, Fe^{2+} ions were attracted onto the surface of TGs and finally formed the $FePO_4$/graphene hybrids which were then annealed at 350 °C for 3 h to remove the hydrated water (Scheme 1c).

As-synthesized $FePO_4$/graphene hybrids were used to fabricate $LiFePO_4$/graphene hybrids. Such composites were well mixed with the $LiCH_3COOH$ using vacuum pressure infiltration. The obtained mixtures were subsequently fired in an argon atmosphere at 700 °C for 10 h and finally acquired the $LiFePO_4$/graphene hybrids (Scheme 1d). As a control group, pristine $FePO_4$ and $LiFePO_4$ were prepared using the same method without graphene nanosheets and RAAP added.

The morphology and structure of the samples were characterized by transmission electron microscopy (TEM, FEI Tecnai F20 S-Twins) and scanning electron microscope (SEM, Hitachi S-4800) with energy-dispersive X-ray spectroscopy (EDS, Phoenix). X-ray diffraction (XRD) analysis was performed on a D/Max-RA X-ray diffractometer and Raman spectra was recorded by a Renishaw in via spectrometer with excitation at 514.5 nm provided by Ar^+ laser. XPS measurements were acquired with a monochromatic Al Kα X-ray source on a PHI 5000 Versa Probe XPS spectrometer. The carbon content in the $FePO_4$/graphene composites was measured using a Heraeus CHN–O–Rapid elemental analyser as 6.8 wt% in the whole sample and the carbon content in the $LiFePO_4$/graphene was measured with the same method as 6.2 wt%.

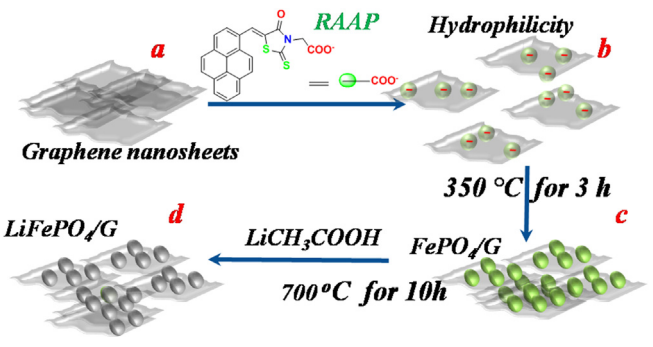

Scheme 1. Illustration of the procedures for preparation of $FePO_4$/graphene and $LiFePO_4$/graphene hybrids.

For the cathode preparation, $FePO_4$/graphene and $LiFePO_4$/graphene hybrids were admixed with poly vinylidene fluoride (PVDF) in a weight ratio of 10:1, the mixture was spread and pressed onto a porous Al-mesh, followed by overnight drying at 100 °C in vacuum; As for the control group, the pristine $FePO_4$ cathode and $LiFePO_4$ cathode were prepared by mixing 80% of active material (pristine $FePO_4$ or $LiFePO_4$), 5% carbon black, 5% graphene nanosheets and 10% PVDF dispersed in N-methylpyrrolidinone (NMP). The homogenous slurries were coated on an Al-foil and then dried at 100 °C for 10 h. All of the charge–discharge tests were performed in a land battery cycler with voltage of 2.0–4.2 V and the electrochemical impedance spectroscopy (EIS) measurements were carried out on a CHI660-C potentiostat/galvanostat (Shanghai Chenhua Technology Inc., China).

3. Results and discussion

The thermal reduced TGs reveal an “accordion-like” structure which consists of many highly-wrinkled graphene sheets as shown in Fig. 1a. Such composites are well decorated with the dispersant RAAP in the DMF/water solution, Fig. 1b shows the SEM image of the highly dispersed RAAP decorated TGs. From the pattern, the exfoliated graphene sheets are well separated from each other because of the strong hydrophilicity. The morphology of as-prepared $FePO_4$/graphene hybrids is shown in Fig. 1c. It can be seen that a large quantity of $FePO_4$ particles are attached into the TGs. Fig. 1d shows more details about the hybrids. The amorphous $FePO_4$ particles are uniform distributed on the high dispersed exfoliated graphene sheets; most of the graphene wrapped particles show sphere-like morphology. The elemental analysis of the composite carried out by EDS is shown in Fig. 1e, proving that components of $FePO_4$ as the ratio of Fe: P is near 1:1. Fig. 1f and Fig. S1 (shown in the Supplementary material) shows the morphology of the $LiFePO_4$/graphene hybrids transformed from as-prepared $FePO_4$/graphene composites. After the thermal reduction process, the morphology and particle size of thus obtained $LiFePO_4$/graphene composites were in general similar to those of the $FePO_4$/graphene precursor. This result clearly indicated that the thermal reduction process did not significantly change the hybrid structure of the precursors and thus retained the well connection between the $LiFePO_4$ nanospheres and flexible conductivity graphene sheets.

The crystallographic structures of the as-prepared $FePO_4$/graphene and $LiFePO_4$/graphene hybrids were further examined by X-ray diffraction (XRD). As shown in XRD pattern of $FePO_4$/graphene hybrids in Fig. 2a, no diffraction peaks of $FePO_4$ but only a broad peak between 20 and 40° is observed, corresponding to the graphene nanosheets [18]. This amorphous feature of $FePO_4$ is anticipated because of the low synthesis temperature (350 °C) [4]. Fig. 2b shows the XRD plot of as-synthesized $LiFePO_4$/graphene hybrids. All the diffraction peaks can be well indexed to the orthorhombic $LiFePO_4$ phase with the space group of Pnma, indicating thermal reduction strategy can acquire pure olive phase $LiFePO_4$ [18]. The Raman spectrums of $FePO_4$/graphene and $LiFePO_4$/graphene hybrids are shown in Fig. 2c and d. From the patterns, $FePO_4$/graphene and $LiFePO_4$/graphene hybrids show similar Raman spectra as two broad peaks at ~1351 and ~1600 cm^{-1} which can be assigned to the D and G peaks of graphene [14,24,25]. Both hybrids show stronger G band compared to D band indicating such hybrids show highly ordered graphene structure. The intensity of I_D/I_G of $FePO_4$/graphene and $LiFePO_4$/graphene hybrids are 0.76 and 0.72, indicating the thermal reduction process can improve graphitization degree of the hybrids. It should be pointed out that the width at half-maximum of both the D band and G band for the $LiFePO_4$/graphene is apparently smaller than that of $FePO_4$/graphene, suggesting that the graphene sheets of the $LiFePO_4$/graphene hybrids

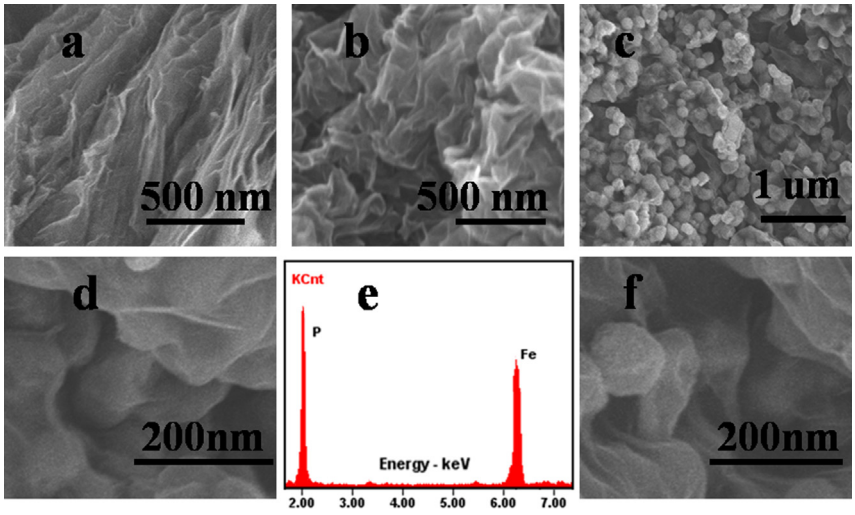

Fig. 1. (a) SEM image of the TGs. (b) SEM image of the high-dispersed RAAP decorated TGs. (c)–(d) SEM images of the $FePO_4$/graphene hybrids. (e) EDS result of the $FePO_4$/graphene hybrids. (f) SEM image of the $LiFePO_4$/graphene hybrids.

has a higher degree of graphitization than that of $FePO_4$/graphene hybrids [26]. X-ray photoelectron spectroscopy (XPS) analysis was carried out to analyze the valence states change of Fe elements and possible interaction between $LiFePO_4$ and graphene. After thermal reduction process, the binding energy of $Fe2p_{3/2}$ moves from 712 eV to 710 eV, corresponding to the valence change from Fe (III) state to Fe (II) in the samples (Fig. S2a) [18]. Fig S2b shows the C1s of as-synthesized $LiFePO_4$/graphene hybrids, the binding energy of C–C appears at a value of 284.1 eV, which is smaller than the standard value as 284.6 eV. This may be ascribed to the charge transfer between $LiFePO_4$ and graphene.

To further examine the hybrid structure of $LiFePO_4$/graphene hybrids, the TEM images are provided in Fig. 3a and b. It can be seen that the $LiFePO_4$ nanospheres are directly grown on the graphene-assembled scaffold which gives a well interconnected, 3-D conductive network channel in the $LiFePO_4$/graphene composites. The size distribution of the $LiFePO_4$ particles is between 40 and 70 nm (Fig. S3). Such structure can efficiently enhance the electronic conductivity and structural stability of the whole hybrids, leading to improved electrochemical properties which will be discussed later. Fig. 3c as the high-resolution TEM (HRTEM) image of the $LiFePO_4$ nanospheres reveals the presence of a thin carbon shell between the nanoparticles and TGs which can also be found in Fig. 3d. Such structures can efficient collect electrons from the $LiFePO_4$ to the high conductive TGs.

The as-prepared $FePO_4$/graphene and $LiFePO_4$/graphene cathode materials were assembled into coin cells to evaluate their electrochemical performances. Electrochemical impedance spectroscopy (EIS) was applied to measure the impedance spectra of the $FePO_4$/graphene and $LiFePO_4$/graphene hybrids. Fig. S4 shows the Nyquist plots of $FePO_4$/graphene and $LiFePO_4$/graphene with their control groups. All impedance curves show one compressed

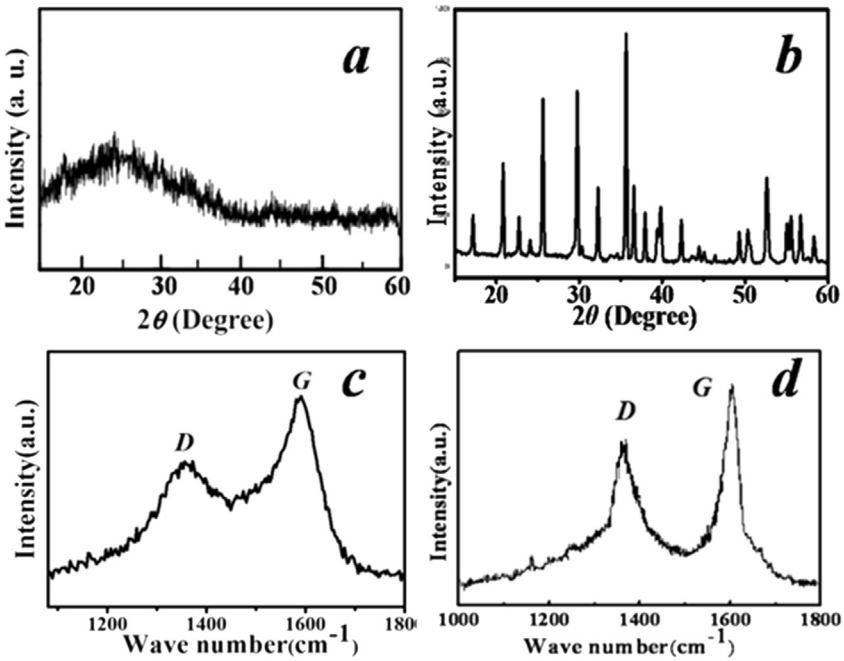

Fig. 2. XRD pattern of the $FePO_4$/graphene (a) and $LiFePO_4$/graphene (b) hybrids; Raman spectra of $FePO_4$/graphene (c) and $LiFePO_4$/graphene (d) hybrids.

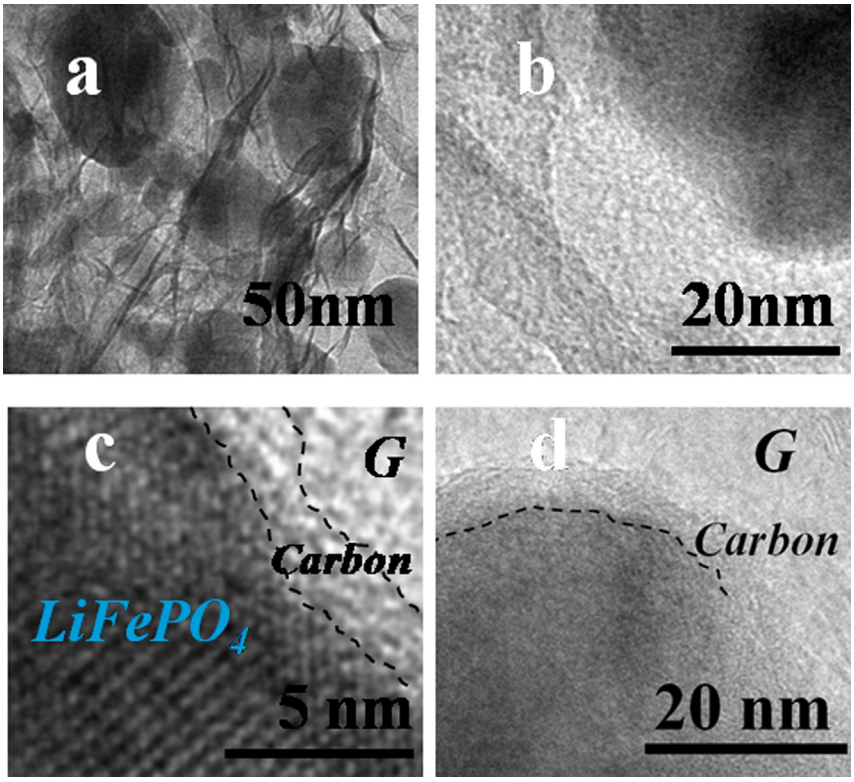

Fig. 3. (a)–(b) TEM image of the $LiFePO_4$/graphene hybrids. (c) HRTEM result of the $LiFePO_4$/graphene hybrids. (d) TEM image shows carbon shell on the surface of $LiFePO_4$ particle.

semicircle in the medium-frequency region, which could be assigned to the charge-transfer resistance (R_{ct}). Apparently, the diameter of the semicircles for $FePO_4$/graphene and $LiFePO_4$/graphene hybrids is significantly smaller than the control groups, indicating the graphene decorated hybrids possess lower contact and charge-transfer impedance [27]. Fig. 4a shows the charge/discharge profiles of the $FePO_4$/graphene cathode in a potential window of 2.0–4.2 V (versus Li^+/Li). The potential increases (or decreases) smoothly as a function of the state of charge (or discharge), which is similar to the reported $FePO_4$-based batteries. Such battery shows a high reversible capacity as 166 mAh g^{-1} at the first cycle (0.2 C, 1C = 178 mA g^{-1}) and then stabled at 163 mAh g^{-1}. With an increase in the current rate, the hybrid cathode exhibited excellent rate capacity as 150 mAh g^{-1} at 1 C, 134 mAh g^{-1} at 4 C

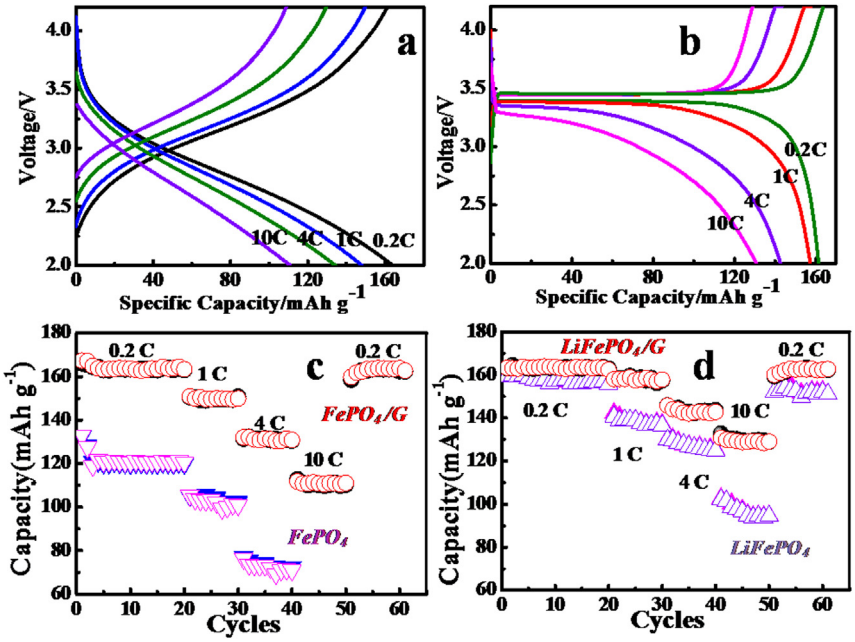

Fig. 4. Representative discharge–charge curves at various current rates of (a) $FePO_4$/graphene and (b) $LiFePO_4$/graphene-based LIBs. Cycle performance at different C-rates of (c) $FePO_4$/graphene and (d) $LiFePO_4$/graphene-based LIBs.

and 112 mAh g^{-1} of 10 C, respectively, demonstrating that the rate capability of as-synthesized $FePO_4$/graphene cathode is much better than the previously reported work [18]. Electrochemical performance of as-prepared $LiFePO_4$/graphene cathode was also studied to confirm the advantage of such hybrid structure (Fig. 4b). The electrode delivers a discharge capacity of 164 mAh g^{-1} (0.2 C, 1C = 169 mA g^{-1}) with a voltage plateau near 3.4 V which is close to the theory capacity of $LiFePO_4$. As the rate increased from 1 C to 10 C, an excellent rate performance is acquired as 158 mAh g^{-1} at 1 C, 142 mAh g^{-1} at 4 C and 131 mAh g^{-1} at 10 C, which is one of the best results among the reported graphene decorated $LiFePO_4$ cathodes [13,14,28]. The outstanding electrochemical properties of $FePO_4$/graphene and $LiFePO_4$/graphene cathodes are believed to be associated with the unique structure of the nano-sized particles, high conductive TGs and their tightly-bonded interfaces which provide a short ion diffusion distance and good electron conduction in such hybrids.

The more remarkable advantage of such $FePO_4$/graphene and $LiFePO_4$/graphene hybrids of LIBs is the cycle performance at different C-rates. Both samples present excellent cycle stability with large rate capacity as shown in Fig. 4c and d. The pristine $FePO_4$ cathode as the control group shows a poor rate capacity at 4 C as 73–68 mAh g^{-1}; In contrast, $FePO_4$/graphene hybrids can achieve 132–130 mAh g^{-1} at 4 C and 112–109 mAh g^{-1} at 10 C (Fig. 4c). Fig. 4d shows the specific discharge capacities vs. cycle number at various current rates for $LiFePO_4$/graphene hybrids and the pristine $LiFePO_4$. At a given low current rate as 0.2 C, $LiFePO_4$/graphene-battery delivers 165–163 mAh g^{-1} while the control group acquires a comparable capacity of 160–157 mAh g^{-1}. However, as the current rate increases, the cell prepared with $LiFePO_4$/graphene hybrids scored obviously better than the latter one. For example, the reversible capacity of the $LiFePO_4$/graphene hybrids could achieved 145–142 mAh g^{-1} at 4 C and 131–129 mAh g^{-1} at 10 C, whereas the graphene-free sample only shows 128–125 mAh g^{-1} at 4 C and 102–94 mAh g^{-1} at 10 C. The improved cycle ability of both $FePO_4$/graphene and $LiFePO_4$/graphene-based batteries may be attributed to the enhancement of electronic conductivity of the TGs and short ion diffusion paths of the nano-sized particles. It should be also pointed out that the original discharge capacity of $FePO_4$/graphene and $LiFePO_4$/graphene hybrids can be recovered after cycled at high current rates, demonstrating that such hybrid architectures are tolerant to varied charge and discharge currents, which is a highly desirable property for electrode materials in lithium ion batteries [15,16,29,30,31].

4. Conclusion

In summary, we have reported a RAAP-direct growth method to fabricate $FePO_4$/graphene and $LiFePO_4$/graphene hybrids. $FePO_4$ spheres were directly grown on the surface of high-dispersed TG-assembled scaffolds which was functionalized by RAAP without pre-oxidation process, such hybrids can transform to the $LiFePO_4$/graphene hybrids by a thermal reduction method. When evaluated as the cathode material for LIBs, both $FePO_4$/graphene and $LiFePO_4$/graphene exhibit superior performance, i.e., high rate capability combined with good capacity retention upon cycling, due to the unique structure of the composite, including the high conductivity of TGs, nano-sized active materials and well contact between active materials and TGs. Moreover, the simple and eco-friendly fabrication route can easily extended to other graphene-based materials.

Acknowledgments

The authors acknowledge the financial supports of the National Natural Science Fund Committee (21173042, 50602022 and 60808025), National 973 Program (2013CB932902), and Key Laboratory for State Key Laboratory of Silicon Materials Visiting Scholar Fund (SKL2011-17).

Appendix A. Supplementary data

Supplementary data related to this article can be found at http://dx.doi.org/10.1016/j.jpowsour.2014.01.044.

References

[1] J. Liu, X.-W. Liu, Adv. Mater. 24 (2012) 4097–4111.
[2] M. Armand, J.M. Tarascon, Nature 451 (2008) 652–657.
[3] H. Yoo, M. Jo, B.S. Jin, H.S. Kim, J. Cho, Adv. Energy Mater. 1 (2011) 347–351.
[4] S. Okada, T. Yamamoto, Y. Okazaki, J. Yamaki, M. Tokunaga, T. Nishida, J. Power Sources 146 (2005) 570–574.
[5] A. Abouimrane, D. Dambournet, K.W. Chapman, P.J. Chupas, W. Weng, K. Amine, J. Am. Chem. Soc. 134 (2012) 4505–4508.
[6] P. Moreau, D. Guyomard, J. Gaubicher, F. Boucher, Chem. Mater. 22 (2010) 4126–4128.
[7] H. Kim, I. Park, D.-H. Seo, S. Lee, S.-W. Kim, W.J. Kwon, Y.-U. Park, C.S. Kim, S. Jeon, K. Kang, J. Am. Chem. Soc. 134 (2012) 10369–10372.
[8] J. Gao, J. Kim, A. Manthiram, Electrochem. Commun. 11 (2009) 84–86.
[9] X. Zhang, X. Zhang, W. He, Y. Yue, H. Liu, J. Ma, Chem. Commun. 48 (2012) 10093–10095.
[10] Y. Zhou, J. Wang, Y. Hu, R. O'Hayre, Z. Shao, Chem. Commun. 46 (2010) 7151–7153.
[11] Y. Yin, P. Wu, H. Zhang, C. Cai, Electrochem. Commun. 18 (2012) 1–3.
[12] C.X. Guo, Y.Q. Shen, Z.L. Dong, X.D. Chen, X.W. Lou, C.M. Li, Energy Environ. Sci. 5 (2012) 6919–6922.
[13] Y.F. Tang, F.Q. Huang, H. Bi, Z.Q. Liu, D.Y. Wan, J. Power Sources 203 (2012) 130–134.
[14] J.L. Yang, J.J. Wang, D.N. Wang, X.F. Li, D.S. Geng, G.X. Liang, M. Gauthier, R.Y. Li, X.L. Sun, J. Power Sources 208 (2012) 340–344.
[15] X. Guo, Q. Fan, L. Yu, J. Liang, W. Ji, L. Peng, X. Guo, W. Ding, Y. Chen, J. Mater. Chem. A 1 (2013) 11534–11538.
[16] Q. Fan, L. Lei, Y. Chen, Y. Sun, J. Power Sources 224 (2013) 702–706.
[17] Q. Fan, Y. Tang, Y. Chen, J. Power Sources 205 (2012) 463–466.
[18] Y. Yin, Y. Hu, P. Wu, H. Zhang, C. Cai, Chem. Commun. 48 (2012) 2137–2139.
[19] S.-W. Kim, J. Ryu, C.B. Park, K. Kang, Chem. Commun. 46 (2010) 7409–7411.
[20] J.-P. Jegal, J.-G. Kim, K.B. Kim, Electrochem. Commun. 30 (2013) 87–90.
[21] Y. Liu, Y. Xu, X. Han, C. Pellegrinelli, Y. Zhu, H. Zhu, J. Wan, A.C. Chung, O. Vaaland, C. Wang, Nano Lett. 12 (2012) 5664–5668.
[22] L. Chen, P. Wu, K. Xie, J. Li, B. Xu, G. Cao, Y. Chen, Y. Tang, Y. Zhou, T. Lu, Electrochim. Acta 92 (2013) 433–437.
[23] N. Li, M. Zheng, H. Lu, Z. Hu, C. Shen, X. Chang, G. Ji, J. Cao, Y. Shi, Chem. Commun. 48 (2012) 4106–4108.
[24] X. Rui, D. Sim, K. Wong, J. Zhu, W. Liu, C. Xu, H. Tan, N. Xiao, H.H. Hng, T.M. Lim, Q. Yan, J. Power Sources 214 (2012) 171–177.
[25] J.Z. Wang, C. Zhong, S.L. Chou, H.K. Liu, Electrochem. Commun. 12 (2010) 1467–1470.
[26] X.F. Zhou, F. Wang, Y.M. Zhu, Z.P. Liu, J. Mater. Chem. 21 (2011) 3353–3358.
[27] X.L. Wu, Y.G. Guo, J. Su, J.W. Xiong, Y.L. Zhang, L.J. Wan, Adv. Energy Mater. 3 (2013) 1155–1160.
[28] Y. Zhang, W.C. Wang, P.H. Li, Y.B. Fu, X.H. Ma, J. Power Sources 210 (2012) 47–53.
[29] Q. Fan, Y.F. Chen, J. Nanosci. Nanotechnol. 12 (2012) 3979–3983.
[30] Q. Fan, L.X. Lei, G. Yin, Y.F. Chen, Y.M. Sun, Electrochem. Commun. 38 (2014) 120–123.
[31] Q. Fan, L.X. Lei, G. Yin, Y.M. Sun, Chem. Commun. (2014), http://dx.doi.org/10.1039/C3CC48367C.